The direct simulation Monte Carlo method using unstructured adaptive mesh and its application

J.-S. Wu[*,†], K.-C. Tseng and C.-H. Kuo

Department of Mechanical Engineering, National Chiao-Tung University, Hsinchu 30050, Taiwan

SUMMARY

The implementation of an adaptive mesh-embedding (*h-refinement*) scheme using unstructured grid in two-dimensional direct simulation Monte Carlo (DSMC) method is reported. In this technique, local isotropic refinement is used to introduce new mesh where the local cell Knudsen number is less than some preset value. This simple scheme, however, has several severe consequences affecting the performance of the DSMC method. Thus, we have applied a technique to remove the hanging node, by introducing the an-isotropic refinement in the interfacial cells between refined and non-refined cells. Not only does this remedy increase a negligible amount of work, but it also removes all the difficulties presented in the originals scheme. We have tested the proposed scheme for argon gas in a high-speed driven cavity flow. The results show an improved flow resolution as compared with that of un-adaptive mesh. Finally, we have used triangular adaptive mesh to compute a near-continuum gas flow, a hypersonic flow over a cylinder. The results show fairly good agreement with previous studies. In summary, the proposed simple mesh adaptation is very useful in computing rarefied gas flows, which involve both complicated geometry and highly non-uniform density variations throughout the flow field. Copyright © 2002 John Wiley & Sons, Ltd.

KEY WORDS: DSMC; adaptive mesh; mesh refinement; Knudsen number; driven cavity flow; cylinder flow

I. INTRODUCTION

Rarefied gas dynamics

The highly developed computational fluid dynamics (CFD) using the Navier–Stokes equations has permitted the prediction of complex thermal and fluid problems of engineering and scientific interest. However, there are limitations to the applicability based on these equations. In some flow regimes, the Navier–Stokes equations fail to approximate the gas dynamics behaviour and the particle nature of the matter must be taken into account. One of these is the rarefied gas flow, which the mean free path becomes comparable with, or even larger than,

---
[*] Correspondence to: Dr. J.-S. Wu, Department of Mechanical Engineering, National Chiao-Tung University, 1001 Ta-Hsueh Road, Hsinchu 30050, Taiwan.
[†] E-mail: chongsin@cc.nctu.edu.tw

the characteristic length of flows. Such flows can be characterized by the Knudsen number, $Kn = \lambda/L$, where λ is the mean free path, and L is the characteristic length. Knudsen number is usually used to indicate the degree of rarefaction. Traditionally, flows are divided into four regimes as follows [1]: $Kn < 0.01$ (continuum), $0.01 < Kn < 0.1$ (slip flow), $0.1 < Kn < 3$ (transitional flow) and $Kn > 3$ (free molecular flow). As the Kn increases, the rarefaction becomes important and even dominates the flow behaviour. Hence, the N-S based CFD techniques are often inappropriate for higher Kn flows, such as slip flow, transitional flow and free-molecular flow.

Solution methodologies

The understanding of the rarefied gas dynamics (high Knudsen number flows) has played or began to play an important role in several research disciplines. Each of these applications of high Knudsen number flows is now of practical scientific and engineering importance. While the Boltzmann equation may be more suitable for approximating high Knudsen number flows, attempts to solve it numerically have met with much less success than the Navier–Stokes equations due to the higher dimensionality (up to seven) of the Boltzmann equation and the difficulties of modelling the integral collision term. To circumvent the difficulty of a direct solution of the Boltzmann equation, an alternative method known as direct simulation Monte Carlo (DSMC) was proposed by Bird [2] in 1963 to compute the hypersonic flows. Further applications of the DSMC method include gas flows around spacecraft [3, 4], pumping characteristics of high vacuum pump [5, 6], conductance computation of an orifice [7], the slider air bearing of the computer hard disk [8] and, recently, the micro-scale gas flows [9–11], among others. This method requires the introduction of computational cells (meshes) similar to those in CFD; however, the cells are mainly used for selecting collision partners, sampling and averaging the macroscopic flow properties. Many physical problems involve very complicated geometry or highly non-uniform density variations throughout the flow field; hence, the generation of an appropriate mesh often becomes a very demanding and time-consuming task. Generally, the appropriate mesh used for final computation is obtained through trials and errors. In addition, the sizes of cell used in the DSMC method have to vary according to the density or have to be refined near the body surface to obtain accurate prediction of pressure, friction and heat transfer; however, these are not known as *a priori* in general.

Structured and unstructured mesh

Most applications of DSMC applied *structured mesh* [12] in the physical space. For problems with complicated geometry, multi-block meshing techniques were developed first by Bird [2, 12], which involved two steps: dividing the flow field into several blocks followed by discretizing each block into quadrilateral (2D) or cubic (3D) mesh. Subsequent research has developed alternative meshing techniques such as the coordinate transformation method by Merkle [13], the body-fitted coordinate system by Shimada and Abe [14] and the transfinite interpolation method by Olynick *et al.* [15]. All of these still used structured grids. It is much easier to program the code using structured grids; however, it requires tremendous problem-specific modification. To alleviate such restriction and considering the efficiency of applying the mesh adaptation, *unstructured mesh* should be the best choice, although it might be computationally more expensive. Boyd and his coworkers [3, 4] have applied such a technique to compute the thruster plume produced by spacecraft and found that the results are very

satisfactory. In addition, several studies [9, 11] have used such a technique to compute micro-scale flows, including the micro-channel, the micro-nozzle, the slider air bearing of computer hard disk and the micro-manifold.

Mesh adaptation

The development of mesh adaptation in CFD and DSMC are described in the following in turn.

CFD For the past decade, the development of CFD using adaptive unstructured meshes has greatly extended the capability of predicting complex flow fields. Several adaptive mesh techniques have been developed to increase the resolution of 'important' region and decrease the resolution of 'unimportant' region within the flow field, as reviewed by Powell *et al.* [16].

In general, mesh adaptation can be categorized into three methods [17]: (1) re-meshing (mesh generation), (2) mesh movement, and (3) mesh enrichment (or *h-refinement*). For the first method, a solution based on the initial mesh is obtained, and then the mesh is regenerated, which the mesh points are more concentrated on where resolution of the solution is needed. This new mesh may contain more or fewer mesh points than the original mesh. For the second method, the total mesh points remain the same in the computational domain. It is common to use a spring analogy, in which the nodes of the mesh are connected by springs whose stiffness is proportional to certain measure of solution activity over the spring. The mesh points are moved closer into the region where solution gradients are relatively large. This is often applied to the spatial adaptation of a structured mesh. For the final method, mesh enrichment, mesh points are added or embedded into the regions where relatively large solution gradients are detected, while the global mesh topology remains intact. It is generally regarded that mesh enrichment method has certain advantages over the first two methods [17, 18]. One of the most important advantages is that the mesh enrichment technique is in general many times faster and robust than the re-meshing technique [18]. In Reference [17], it is mentioned that the disadvantage, however, is that the implementation of mesh enrichment involves a significant modification to existing numerical schemes due to the appearance of hanging nodes. This can be easily overcome, however, by some simple methods through the elimination of hanging nodes, as proposed by Kallinderis and Vijayan [19].

DSMC The corresponding development and the application of the adaptive mesh technique in particle method, such as the DSMC method, has been largely ignored. Applying adaptive mesh technique in the DSMC method, as in CFD, not only improves the flow field resolution without increasing the computational cost much, but also more or less equalizes the statistical uncertainties in the averaging process of obtaining the macroscopic quantities.

Among the very few studies about this subject, Wang and Harvey [20] have first applied solution-based, re-meshing adaptive grid technique (mesh regeneration using the advancing front method) in unstructured mesh to study the hypersonic flow field with highly non-uniform density variations involving shocks. Later on in the same group, Robinson [21] has applied a similar technique combining a parallel DSMC method to compute a hypersonic flow over compression ramp at different Knudsen numbers. However, some unexpected results such as lower accuracy for a refined mesh, as compared with a coarse mesh, arose due to smaller particle-per-cell caused by too many cells.

Bohdan [22] developed a technique using the monotonic Lagrangian grid (MLG) in the DSMC method, which provides a time-varying grid system that automatically adapts to local number densities within the flow field. However, the application of this MLG technique to external gas flows is not promising due to the particle sorting problems inhered in the scheme. Additionally, this technique highly restricts the time-step size as compared with the traditional DSMC method, which makes the cost of obtaining the steady-state solution comparably high.

Alejandro and John [23] have developed an adaptive mesh and algorithm refinement (AMAR) embedding the DSMC method within a continuum method (N-S equation solver) at the finest level of an adaptive mesh refinement (AMR) hierarchy. This method can cope with problems possessing several orders of magnitude of length scale.

Concerns related to mesh adaptation

Before implementing the adaptive mesh techniques, several concerns need to be considered as pointed out by the excellent review article by Powell *et al.* [16] and the references cited therein. These concerns are mainly applied to CFD; however, most of these are true to the DSMC method as well. These include the data structure, the initial mesh generation, the mesh adaptation procedure, the adaptation parameters and criteria, and the effect of mesh adaptation on computational algorithm. These are briefly described in turn in the following from the perspectives of the DSMC method.

Data structure There exists a strong relationship between the selected mesh adaptation and the data structure to be used. The majority of the DSMC codes apply structured mesh as mentioned previously. Structured mesh allows the particle tracking to be relatively easy and accesses the mesh information in memory more directly; however, it lacks the flexibility on mesh adaptation. There are two ways of adapting the structured mesh. One way, called *r-refinement*, is to 'distort' the mesh distribution, so that mesh redistributes more crowded in the region where it needs mesh refinement. Another way, called *h-refinement*, is to add mesh in the localized region in both *x*- and *y*-directions; however, it increases unexpectedly the mesh population in other unexpected regions as well, where they are not required at all. To allow for the addition (or deletion) of mesh in the computational domain avoiding the problem outlined in the above, a more sophisticated mesh data structure, rather than the simple structured mesh, has to be adopted. Unstructured mesh cannot be mapped onto a computational space with structured (i, j) indexing. Instead, the connectivity information of mesh has to be stored, which makes the mesh data access indirectly. However, the spawning of the mesh in the regions of interest is much easier as compared to structured mesh due to the un-ordered data structure. It was thus concluded that unstructured mesh is superior to structured mesh considering the advantages and implementation of mesh adaptation.

Initial mesh generation The initial un-adapted mesh required for computation is generated via either advancing front method or Delaunay triangulation if unstructured mesh is used. The detailed description of these two methods can be found in Lohnern and Parikh [24] and Baker [25], respectively, and are not repeated here.

Mesh adaptation procedure We have to decide how to adapt the mesh. For the unstructured mesh, there are generally two ways of adapting the mesh: re-meshing and embedding [20].

For the re-meshing procedure, generation of connectivity information for all the mesh is required at each adaptation step. This is expensive in general as mentioned previously. For the embedding technique, local *h-refinement* is used to introduce new mesh points and only the mesh in the immediate vicinity of new mesh needs to be connected. Hence, it requires less computational effort. In addition, we have also to decide if isotropic or an-isotropic refinement is used. Generally, it is recognized that the quality of the mesh using isotropic refinement is superior to that using an-isotropic refinement.

Adaptation parameters and criteria The decision of where to refine or coarsen the mesh is one of the very critical issues in the mesh-adaptive scheme. For the DSMC method, density is naturally the parameter to be considered. The reason for choosing this parameter is described as follows. It often requires that the computational mesh size is much smaller (at least $1/3 \sim 1/2$) than the local mean free path [2, 12], which is inversely proportional to the local number density. In addition, the choice of density as the adaptation parameter helps equalize the statistical uncertainties due to the sampling process for obtaining the macroscopic quantities.

Effect on computational algorithm The effects of mesh adaptation for DSMC is trivial since the cell is used mainly for selecting collision partners and sampling the particles. Thus, the computational procedure is exactly the same except the cell number increases as mesh adaptation proceeds.

Objectives of the paper

Based on previous reviews, the objectives of the current research are summarized as follows: (1) to develop a general adaptive unstructured mesh enrichment procedure; (2) to test the procedures by performing computation for a high-speed driven cavity flow and assess the efficiency of using density as the adaptation parameter; (3) to determine the accuracy of the adaptive solution by making comparisons with previously studied hypersonic flow over a cylinder.

The paper begins with descriptions of the DSMC method with mesh adaptation. Results are then considered treating benchmark test using a driven cavity flow and its applications to a hypersonic flow in turn.

II. THE DSMC METHOD WITH MESH ADAPTATION

As mentioned previously, to achieve higher resolution of flow properties, it is necessary to adapt the existing mesh to the flow conditions. Thus, in the current section, the general features of the proposed DSMC method with mesh adaptation will be described in detail. This section begins with the brief introduction (review) of the conventional DSMC method and then the detailed procedure of proposed mesh adaptation is outlined at the end.

The conventional DSMC method

The basic idea of DSMC is to calculate practical gas flows through the use of no more than the collision mechanics. The molecules move in the simulated physical domain so that the physical time is a parameter in the simulation and all flows are computed as unsteady

flows. An important feature of DSMC is that the molecular motion and the intermolecular collisions are uncoupled over the time intervals that are much smaller than the mean collision time. Both the collision between molecules and the interaction between molecules and solid boundaries are computed on a probabilistic basis and, hence, this method makes extensive use of random numbers. In most practical applications, the number of simulated molecules is extremely small compared with the number of real molecules. The details of the procedures and the consequences of the computational approximations can be found in Bird [2, 12]. In the current study, the variable hard sphere (VHS) model [12] and the no time counter (NTC) method [12] were used to simulate the molecular collision kinetics.

The macroscopic quantities such as mean velocities and temperatures are sampled and averaged from cells, which may be triangular or quadrilateral or hybrid with both. Because of the unstructured mesh used, cell-by-cell particle tracing technique using the cell connectivity information, similar to Piekos and Breuer [9], was adopted to locate the final particle position at the end of each time step during computation. It offered the greatest flexibility of handling different types of boundary conditions and required much less specific problem change in programming. In addition, the mesh adaptation described later also benefits greatly from the use of unstructured mesh.

The DSMC method with mesh adaptation

General features Based on the reviews in previous chapter and considering the application to DSMC, the general features of an adaptive mesh generation scheme are proposed as follows: (1) unstructured mesh (triangular or quadrilateral or hybrid); (2) *h-refinement* with mesh embedding; (3) local cell Knudsen number (inversely proportional to density) and free-stream parameter (relative local density ratio to free-stream value) as the mesh adaptation parameters; (4) upper limit on maximum number of levels of mesh adaptation.

Adaptation parameters and criteria All mesh adaptation methods need some means to detect the requirement of local mesh refinement to better resolve the features in the flow fields and hence to achieve more accurate numerical solutions. This also applies to DSMC. It is important for the adaptation parameters to detect a variety of flow features but does not cost too much computationally. Often gradient of properties such as pressure, density or velocity is used as the adaptation parameter to detect rapid changes of the flow-field solution in traditional CFD. However, by considering the statistical nature of the DSMC method, density is adopted instead as the adaptation parameter. Using density as the adaptation parameter in DSMC is justified since it is generally required that the mesh size be much smaller than the local mean free path to better resolve the flow features, as mentioned previously.

To use the density as an adaptation parameter, a local cell Knudsen number is defined as

$$Kn_c = \frac{\lambda_c}{\sqrt{A_c}} \qquad (1)$$

where λ_c is the local cell mean free path based on HS model and A_c is the magnitude of local cell area. When the mesh adaptation module is initiated, local Knudsen number at each cell is computed and compared with a preset value, Kn_{cc}. If this value is less than the preset value, then mesh refinement is required. If not, check the next cell until all cells are checked. This adaptation parameter is expected to be most stringent on mesh refinement (more cells

1 hanging node
(b)

2 hanging nodes
(c)

initial grid
(a)

—————— isotropic   (1st stage)
—————— isotropic   (2nd stage)
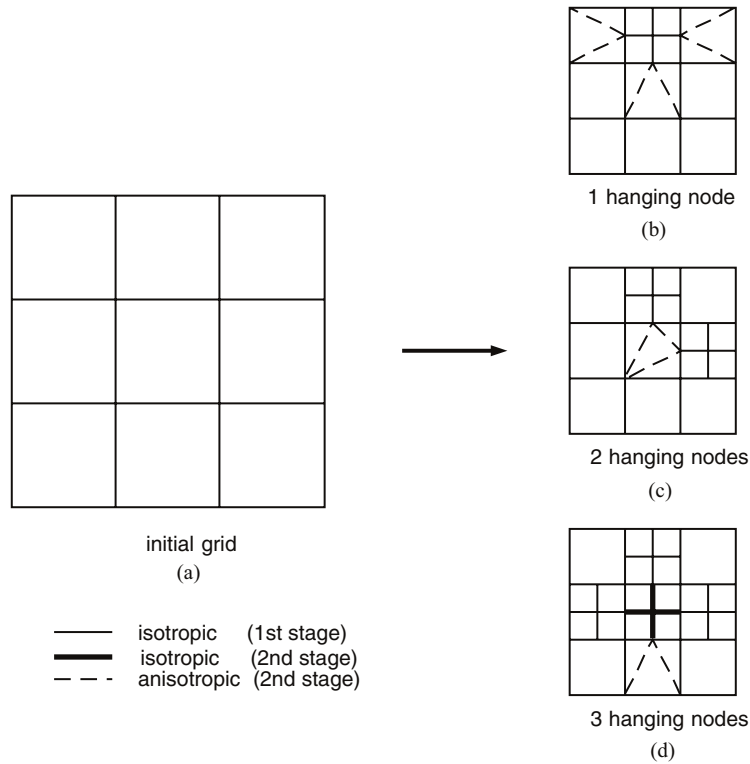– — – anisotropic (2nd stage)

3 hanging nodes
(d)

Figure 1. Mesh refinement rules for quadrilateral cell.

are added); hence, the impact to DSMC computational cost might be high, but is required to obtain an accurate solution.

Considering the practical applications of mesh adaptation in external flows, we have added another constraint, $\phi \geqslant \phi_0$, where ϕ, free-stream parameter, is defined as

$$\phi = \frac{\rho}{\rho_\infty} \tag{2}$$

and ϕ_0 is a preset value. Not only does the above constraint help to reduce the total refined cell numbers to an acceptable level by reducing the cell numbers in the free-stream region a great deal, but it also reduces the total computational time up to 30 per cent as can be shown later.

Adaptation procedures Before outlining the procedures of mesh adaptation, two general rules are described as follows.

(1) *Isotropic mesh refinement is employed for those cells*, *which flag for mesh refinement*. A new node is added on each edge (face) of a *parent cell* and connecting them to form four *child cells*. This rule applies to quadrilateral and triangular mesh, as illustrated in Figures 1 and 2, respectively. In general, this will create one to three hanging nodes in the interfacial cell, which is not refined, next to the isotropically refined cell. Existence
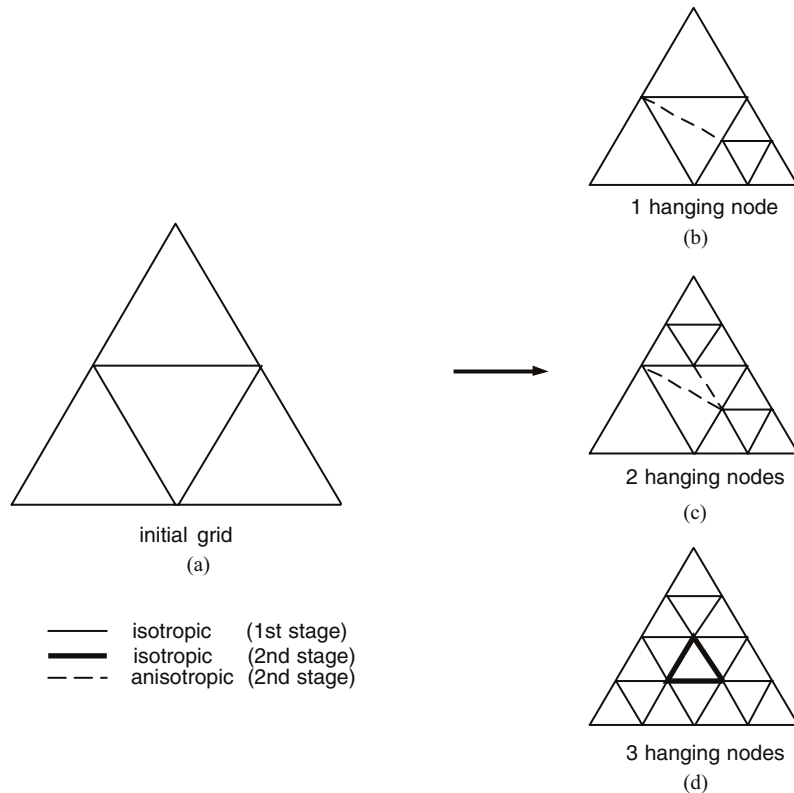
Figure 2. Mesh refinement rules for triangular cell.

of hanging node(s) not only complicates the particle movement, but also increases the cost of the cell-by-cell particle tracing due to the increase of face numbers. Hence, a remedy is proposed as follows in item (2).

(2) *An-isotropic mesh refinement is utilized in the* (*interfacial*) *cells next to those cells that have just been isotropically refined.* Triangular child cells are formed no matter what type the interfacial cell is, considering the generality of the practical programming. Typical methods of interfacial mesh refinement in the quadrilateral and triangular cells are also shown in Figures 1 and 2, respectively. However, some special treatment is required. For example, for a quadrilateral interfacial cell with three hanging nodes (Figure 1(d)), an isotropic cell refinement is conducted and then followed by an an-isotropic mesh refinement in the newly created interfacial cell. The removal of hanging node(s) in the interfacial cells does increase the computational cost; it is, however, trivial as compared with the disadvantages caused by the hanging node(s).

The basic ideas of refining the 2D unstructured mesh, first by isotropic refinement, then by an-isotropic refinement, remain the same for the 3D tetrahedral unstructured mesh, although more complicated conditions will be encountered. Work in this direction will be reported elsewhere in the very near future. In addition, as in most h-refinement processes in CFD,

continuous removal of the hanging node will lead to degenerate triangles. However, the consequence to DSMC is rather different to CFD. In the interfacial regions between refined and unrefined cells (e.g., Figure 10(d)), bad quality cells (large aspect ratio) do occur. In DSMC, this will introduce large errors when particles are collided in the cell if it is treated the same as other normal cells. In our DSMC computation, we have implemented a scheme that if the aspect ratio of the cell is larger than three (or four), then the subcell concept advocated by Bird [12] is used to improve the collision kinetics of particles in the cell. Note that the bad-quality cell numbers are not high as compared with the total cell numbers; hence, the cost increase due to this implementation is minimal.

The mesh adaptation procedures are performed after enough samples of data at each original cell are gathered. As a rule of thumb, about 50 000 particles sampled in a cell are considered enough for the mesh adaptation purpose. The mesh adaptation module is initiated and checks through all the cells to determine if mesh enrichment is required based on the specific adaptation parameter, which was explained previously. If mesh enrichment is conducted, associated neighbour identifying arrays are updated or created, coordinates and number of face for new cells are recorded, and sampled data on the coarse *parent cell* are redistributed (based on the magnitude of cell area) to the finer *child cells* accordingly. The above procedures are repeated until the prescribed maximum number of adaptation levels has been reached or no mesh enrichment is required for all the cells in the computational domain. Before preceding the DSMC computation using the most updated mesh, all sampled data are reset to zero. Finally, the DSMC computation is then conducted on the final refined mesh to accumulate enough samples for obtaining the macroscopic properties in the cells.

In summary, the following steps summarize the procedures for mesh refinement.

(1) Set up initial grids and input data.
(2) Proceed DSMC computation until enough sampled data are gathered at each cell.
(3) Compute the adaptation parameters in each cell using Equations (1) and (2).
(4) Refine all the cells in which both the Kn_c is less than the preset Kn_{cc} and ϕ is large than ϕ_0 by conducting isotropic mesh refinement. If the adaptation criteria are not met, go to step (8).
(5) Create and update the neighbour identifying arrays, coordinates, face numbers, and distribute sampled data to child cells, respectively. Reduce the simulation time step to half.
(6) Check if there are any hanging nodes in the interfacial cells. If there are, then conduct an-isotropic mesh refinement. Also create and update associated cell data as described in step (5).
(7) Return to (2) if both the accumulated adaptation levels are less than the preset maximum value and mesh refinement is required.
(8) If the accumulated adaptation levels are greater than the preset value or no mesh refinement is required, then reset all sampled data to zero and precede the DSMC computation as normal.

The corresponding flow chart is illustrated in Figure 3. Note that the proposed mesh adaptation is capable of refining the mesh close to the body surface following the real surface geometry if the surface contour can be cast into parametric function format as described next.
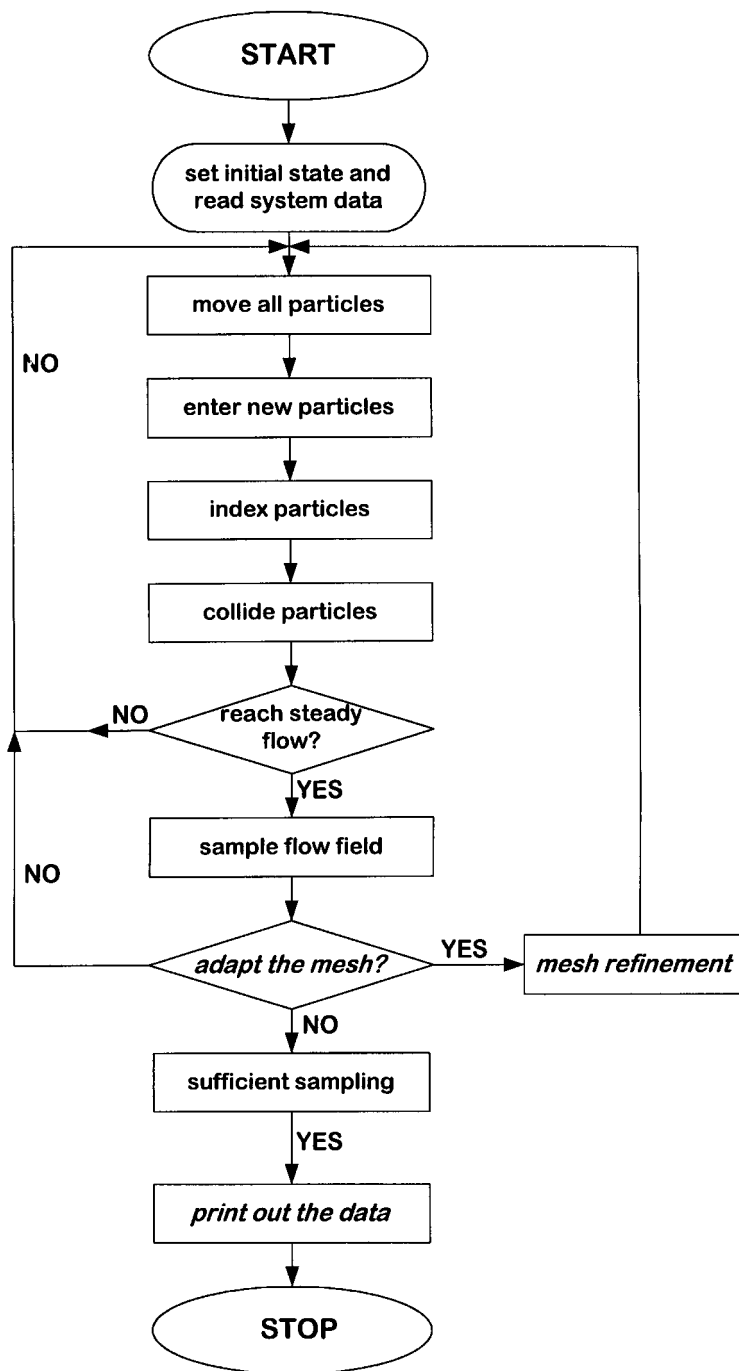
Figure 3. Adaptive-mesh DSMC flowchart.

Surface representation If the boundaries of the computational domain of solid body are not straight, it is not sufficient to place the new node in the midway of the edge (face) of the parent cell. If this is done, a very rough piecewise representation of the original geometry results, which loses the claimed advantages of mesh refinement. What must be done is to move the new node location onto the real boundary contour. In the current implementation, it is assumed that the boundaries can be represented in parametric format. Specific neighbour identifiers are assigned to these non-straight boundary cells to distinguish from straight boundary cells. Whenever the boundary cells, which require mesh refinement, are identified as a non-straight boundary cell, the corresponding parametric function representing the surface contour are called in for mesh refinement to locate the correct node positions along the parametric surface. This can be demonstrated in the application to cylinder flow as shown in the next section.

III. BENCHMARK TEST

A high-speed driven cavity flow is used to verify the mesh adaptation scheme. Note that adaptation criterion is more or less relaxed for the benchmark problem test and results are emphasised on the mesh adaptation rather than the physics of the solution.

Problem description

A high-speed driven cavity flow, as schematically shown in Figure 4, is tested with flow conditions set as follows: $Kn = \lambda_i/H = 0.04$, aspect ratio $L/H = 1$, initial number density $n_i = 6.47E17$, bottom plate speed $V_{\text{plate}} = 8 \times C_{mp}$ and wall temperature $T_w = 300$, where C_{mp} represents the most probable speed based on wall temperature. Initial gas temperatures are 300 K. VHS model is used to model argon gas with molecular data adopted from Bird [12]. This prob-
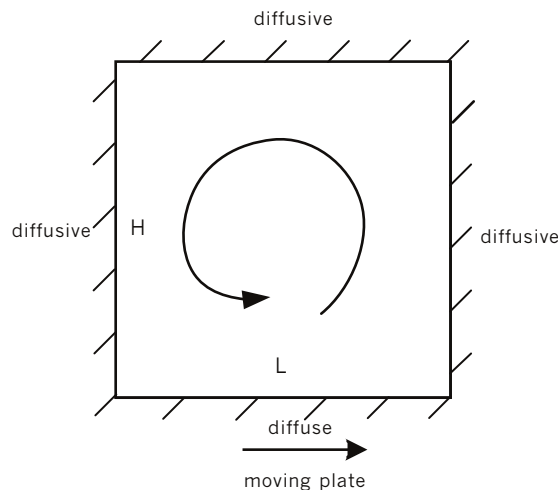

Figure 4. Sketch of a high-speed driven cavity flow ($V_p = 8 \times C_{mp}$, $T_w = 300$ k, Ar gas, $L/H = 1$, $L = 50$ m, $Kn = 0.04$).

lem is chosen as the first test problem due to its simple geometry and expected high-density variations in the cavity.

Simulation results

Results of velocity vector and density ratio (n/n_i) contour, using un-adaptive unstructured quadrilateral mesh (2500 cells) with 62 500 simulated particles, are shown in Figures 5 and 6, respectively. A main counterclockwise circulation, centred at normalised location (0.67, 0.16), is formed within the cavity due to the high-speed moving plate at the bottom. Maximum density ratio $(n/n_i)_{max} = 14.07$ occurs at the right-hand bottom corner of the cavity, while minimum density appears just above the moving plate, both due to the high-speed moving plate at the bottom. These results are considered as the baseline solution for the following results using mesh adaptation.

Quadrilateral and triangular meshes are both used to test the sensitivity of the developed mesh adaptation module; however, only the results using quadrilateral mesh are discussed for this test problem. Note that only local cell Knudsen number (Kn_c) is used as the adaptation parameter for mesh adaptation in the current test problem.

Initial 2500 uniform unstructured quadrilateral cells are used. Corresponding simulation time step is 1.17E-4 seconds. The same particle number (62 500) as that in un-adapted mesh is used. The Kn_c criterion (Kn_{cc}) is set as 0.95. Evolution of adaptive mesh at each level of adaptation is illustrated in Figure 7. As illustrated, the maximum number of mesh adaptation levels is four, although the actual number of adaptation levels is seven. The adaptive mesh for adaptation level greater than four is not shown due to the limited graphic resolution. The number of mesh adaptation levels at the top corners (right- and left-hand) and bottom corner
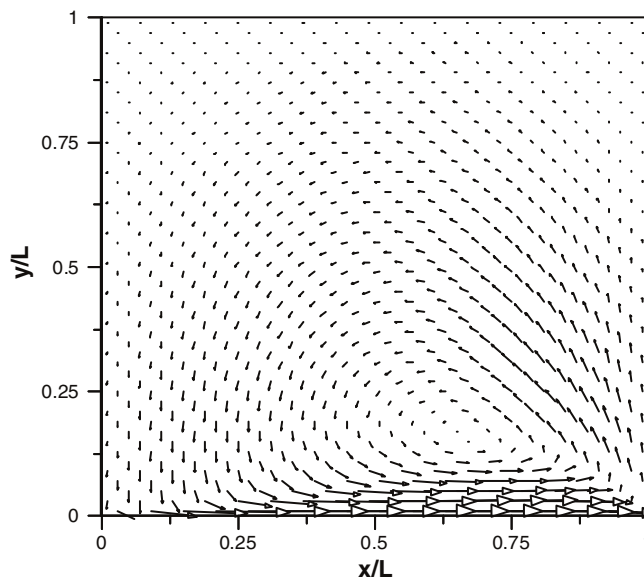

Figure 5. Velocity vectors of a high-speed driven cavity flow using unadaptive mesh ($Kn = 0.04$, 2500 quadrilateral cells).
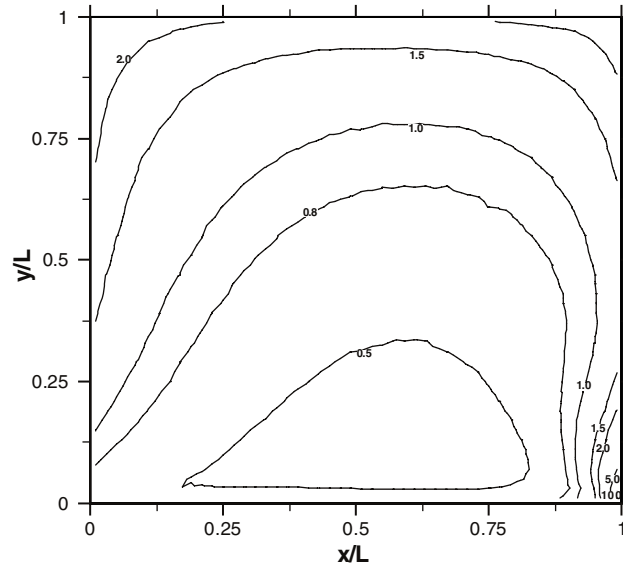
Figure 6. Density ratio of a high-speed driven cavity flow using unadaptive mesh ($Kn = 0.04$, 2500 quadrilateral cells).

(right-hand) are one and seven, respectively. The number of cells increases from 2500 of the original mesh to 2972 of the final refined mesh (level 7). The cell numbers and corresponding minimum Kn_c in the flow field for all adaptation levels are summarized in Table I. Note that the computational penalty caused by mesh adaptation is practically very small as compared with the DSMC computation.

The results of normalised velocity vector and normalised density using the final adaptive mesh (seven levels) are essentially the same as those with un-adaptive mesh. However, a very weak recirculation on the right-hand top corner is resolved due to the refined mesh in this region (not shown). In addition, the maximum density ratio occurs at the right-hand bottom corner increases tremendously up to 160 also due to the very refined mesh in this region. The location of this maximum density ratio does not occur right at the corner cell at the finest cell level, as illustrated in the exploded diagram, Figure 8. This demonstrates that mesh adaptation is important in some regions of the flow where some detailed flow characteristics can only be resolved with very fine grids.

Thus, it is concluded that the proposed solution-based mesh adaptation module is capable of handling both quadrilateral and triangular cells for the high-speed driven cavity flows. Most importantly, the additional computational cost due to mesh adaptation is relatively small as compared with the DSMC computation.

IV. APPLICATION TO REALISTIC FLOW

The proposed mesh adaptation scheme has been verified successfully by the benchmark problems stated previously using the local cell Knudsen number as the adaptation parameter. Thus, to demonstrate the powerful capability of the current mesh adaptation, we have applied it to
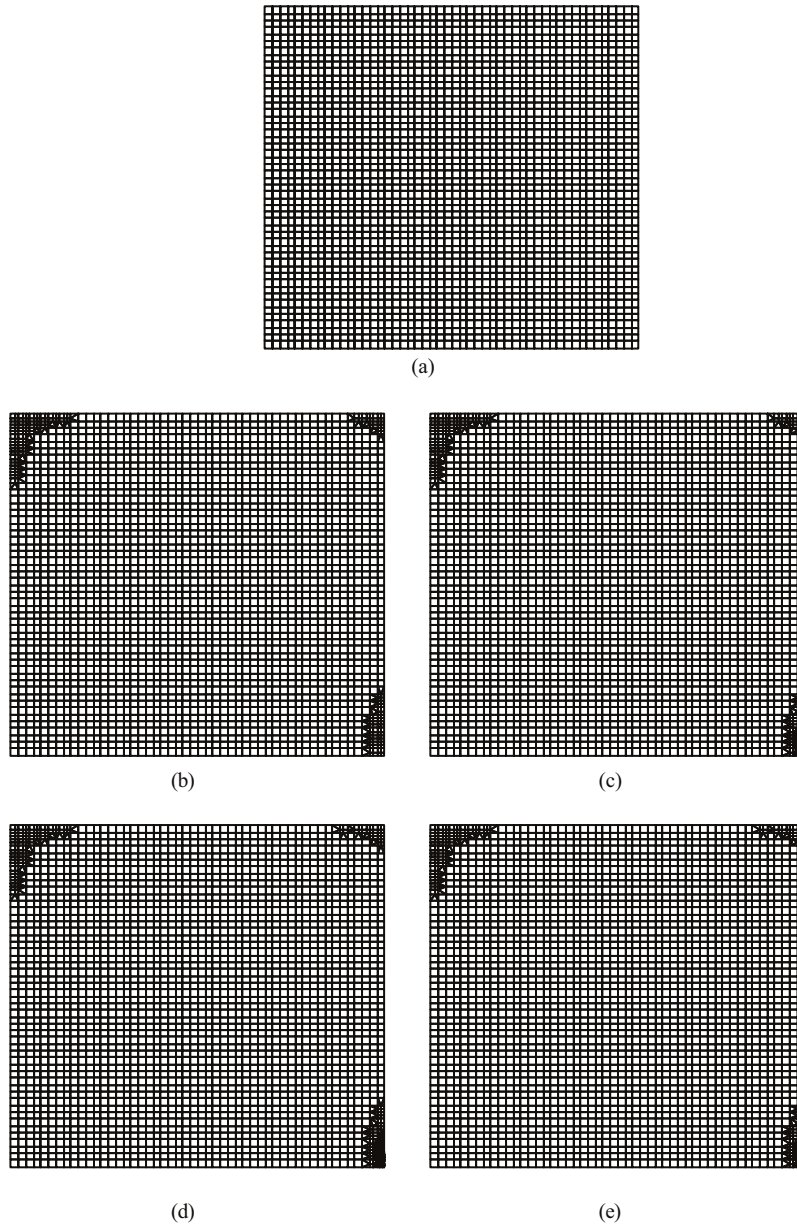
Figure 7. Evolution of unstructured quadrilateral mesh of a high-speed driven cavity flow (a) initial (b) level 1 (c) level 2 (d) level 3 (e) level 4 ($Kn = 0.04$; $Kn_{cc} = 0.95$).

compute a realistic hypersonic flow over a cylinder (Figure 9). The results are then compared with previous simulated or experimental studies available in the literature. Note that the discussion of flow physics will be brief since we are only interested in demonstrating the capability of the current DSMC implementation.

Table I. Total cell numbers and minimum Kn_c at different levels of mesh adaptation for a high-speed driven cavity flow with quadrilateral cells.

Level	0	1	2	3	7
Cell no.	2500	2709	2786	2863	2972
$(Kn_c)_{min}$	0.14	0.194	0.258	0.343	0.954
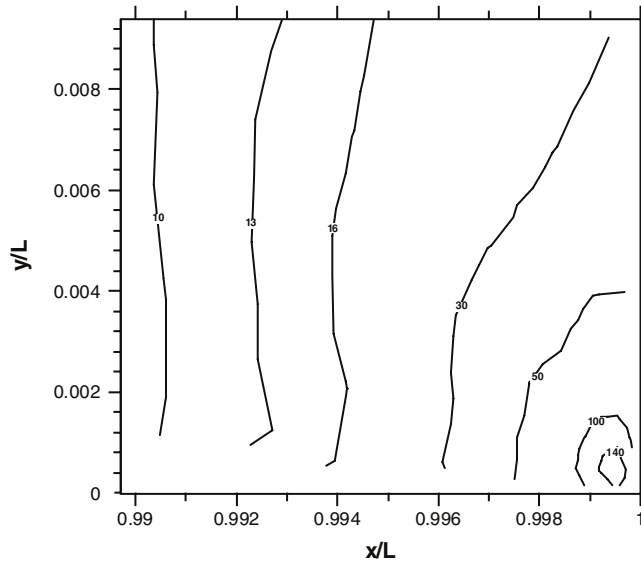
Figure 8. Enlarged view of the density ratio contour using adaptive mesh at the right-hand bottom corner of a high-speed driven cavity flow ($Kn = 0.04$, 2972 quadrilateral cells).
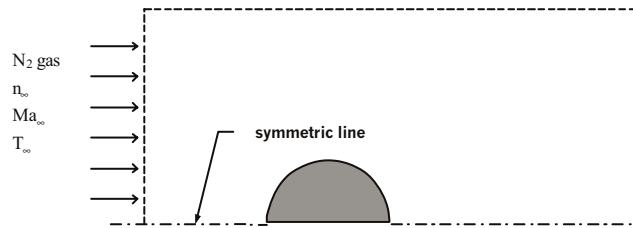
Figure 9. Sketch of a hypersonic flow over a cylinder ($Ma_\infty = 20$, $T_\infty = 20$ K, $n_\infty = 5.1775E19$, N_2 gas, $T_w = 291.6$ K, $D = 1$ m, $Kn_\infty = \lambda/D = 0.025$).

A hypersonic flow over a cylinder

Flow and simulation conditions The flow conditions are listed as follows: VHS nitrogen gas with molecular parameters adopted from Bird [12], free-stream Mach number $M_\infty = 20$, free-stream number density $n_\infty = 5.1775E19$ particles m^{-3}, free-stream temperature $T_\infty = 20$ K, fully thermal accommodated and diffusive cylinder wall with $T_w/T_o = 0.18$, where T_w and

T_o are the wall and the stagnation temperatures, respectively. The corresponding free-stream Knudsen number Kn_∞ ($= \lambda_\infty/D$) and Reynolds number Re_∞ ($= \rho_\infty u_\infty D/\mu_\infty$) is 0.025 and 1834, respectively. These flow conditions represent the experiments conducted by Bütefisch [26]. Parker's temperature-dependent rotational energy exchange model [12] is used to model the diatomic nitrogen gas with the following parametric settings: limiting rotational collision number $Z_r^\infty = 21$, potential well-depth temperature $T^* = 79.8\,\text{K}$.

Mesh adaptation concerns This flow problem is chosen to demonstrate the capability of resolving the expected high density in the stagnation region and the high-density gradient across the detached bow shock around the cylinder. In addition, it also serves to verify the conformation of adaptive mesh to the circular surface. Corresponding adaptation criteria for mesh adaptation is $Kn_{cc} = 1.0$ with maximum number of adaptation levels equal to five. Additional constraint, free-stream parameter, $\phi_0 = 1.05$, which reduces greatly the final refined total cell numbers, is used not to refine those cells with normalised density ratio close to unity (within 5 per cent in this case). The side effect of this constraint might increase the skew of the interfacial cells between un-adaptive free-stream cells and the adaptive cell; however, the reduction of computational cost is appreciable and up to approximately 20–30 per cent. Final free-stream cell size is expected to be much longer than the local mean free path; however, the solution is not expected to deteriorate since nearly uniform flow properties prevail in the free-stream region. The impact on DSMC is minimal as compared with that on CFD since the cells in DSMC are only used for collision and sampling. In addition, initial 5281 triangular cells and approximately 370 000 particles are used for the simulation.

Adaptive mesh and Kn_c contour Evolution of adaptive mesh at each level (only 0–3 shown) is presented in Figure 10 (a)–(d) with $Kn_{cc} = 1.0$ and corresponding results are summarized in Table II. Adaptive mesh for level 4 and 5 are not shown due to the graphic resolution limit such that they look almost the same as level-3 mesh. In Table II, the cell numbers increase from 5281 to 88 959 after five levels of mesh adaptation, while the corresponding minimum Kn_c increases from 0.038 to 0.429. The number of cells is much less than that used by Kuora and Takahira [27], which had 200 000 cells, but the positioning of the cells in the present study may be superior to theirs due to the mesh adaptation scheme applied. As illustrated in Figure 10(a)–(d), the mesh is refined across the strong bow shock around the cylinder (levels 1 and 2) as well as the stagnation region (levels 1–3) in front of the cylinder. It is clear that the proposed mesh adaptation method captures the important flow features such as the bow shock in this case. We would expect that the results in these mesh-refined regions are better than those without mesh adaptation.

Corresponding results of local cell Knudsen number contour at levels 0, 2 and 5 are shown in Figure 11 (a)–(c). It can be seen that Kn_c in the free-stream region remains the same ($Kn_c = 0.54$) after five levels of mesh adaptation, while the Kn_c in both the stagnation region and the shock increases up to $1 \sim 2$. As shown in Table II, the minimum Kn_c is 0.429, which occurs at the interfacial cells behind the shock after level 5. Although the value is less than two or three proposed by Bird [13], the values in most regions of interest (shock and stagnation regions) are very close to or greater than unity. This should improve the flow resolution in these important regions and will be shown clearly when compared with previous studies.
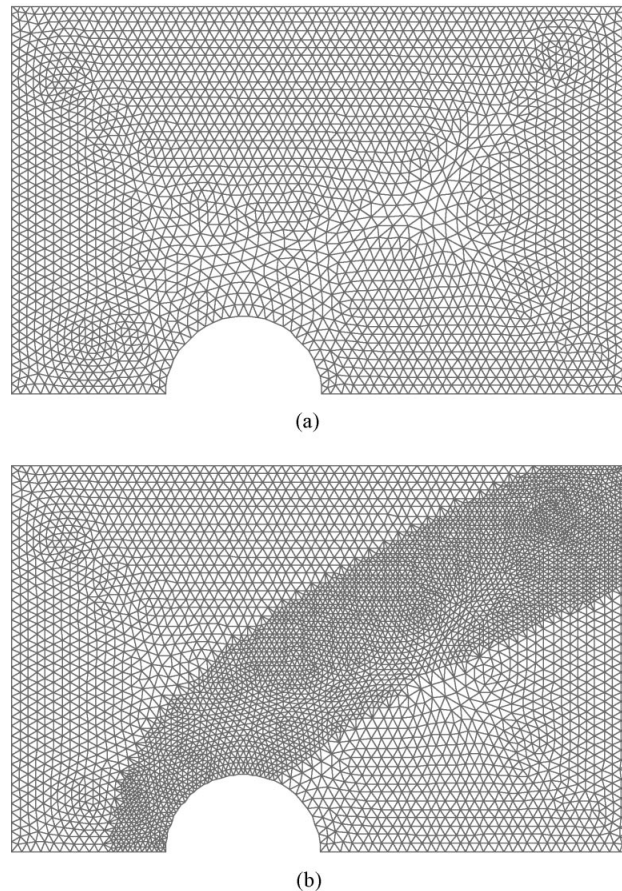
Figure 10. Evolution of unstructured triangular mesh for a hypersonic flow over a cylinder; (a) initial (b) level 1 (c) level 2 (d) level 3 ($Kn_\infty = 0.025$; $Kn_{cc} = 1$; $\phi_0 = 1.05$).

Normalized density contour Results of the normalised density (n/n_∞) are presented in Figure 12. As illustrated, a rather strong bow shock stands off at some distance away from the cylinder. On one hand, the flow is highly compressed across the nearly normal shock to the stagnation point, where density increases tremendously. On the other hand, the flow is slightly compressed across the oblique shock away from the cylinder and then is slightly expanded further downstream. A relatively rarefied region (as compared with free-stream) with the size of cylinder diameter is formed with a density ratio of less than 0.5 behind the cylinder since most gas particles are directed away from the cylinder across the oblique shock as discussed earlier. A maximum value of 26.3 is observed at the stagnation point due to the highly refined mesh in this region, while a minimum value of 0.26 is observed just behind the cylinder.

Non-equilibrium temperature contours The distribution of non-equilibrium between translational and rotational temperatures can be demonstrated clearly by plotting the contour of a
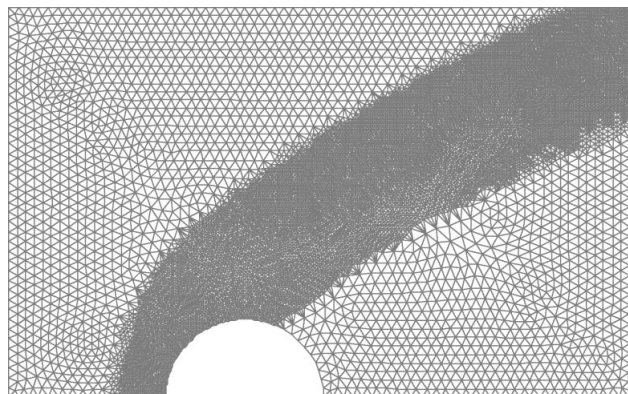
(c)
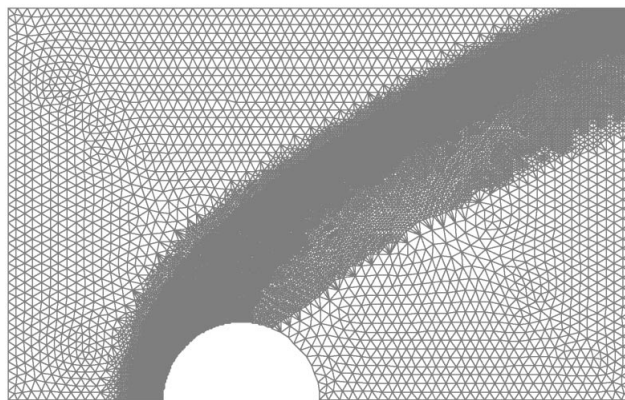
(d)

Figure 10. (*Continued*).

Table II. Total cell numbers and minimum Kn_c at different levels of mesh adaptation for a hypersonic flow over a cylinder with triangular cells.

Level	0	1	2	3	4	5
Cell no.	5281	9938	26646	62328	81762	88959
$(Kn_c)_{min}$	0.038	0.069	0.13	0.246	0.427	0.429

normalised parameter,

$$\psi = |T_{tr} - T_{rot}|/T_{tr}, \tag{3}$$

as presented in Figure 13, where T_{tr} and T_{rot} represent the translational and rotational temperature, respectively. Clearly, strong temperature non-equilibrium exists in the bow shock especially for the regions near the stagnation line. Also appreciable temperature non-equilibrium occurs in the wake and shear layer around the cylinder. In general, the normalised temper-
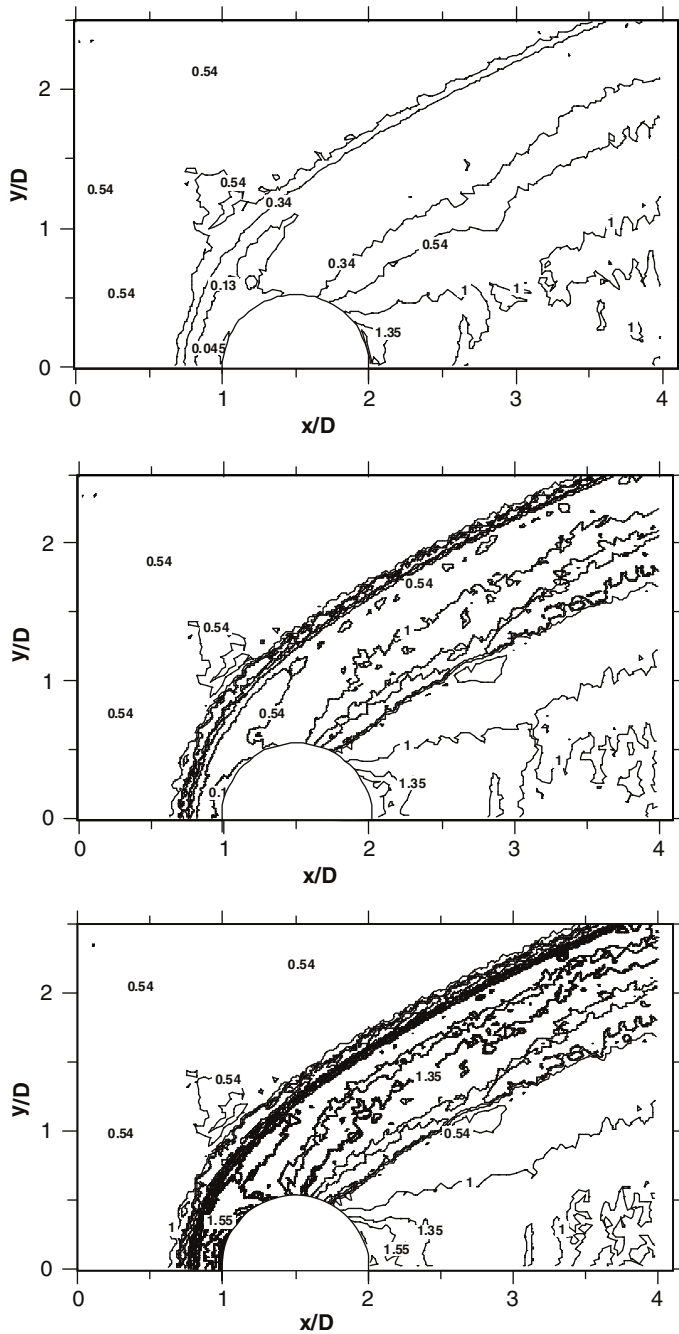
Figure 11. Evolution of local cell Knudsen number for a hypersonic flow over a cylinder; (a) initial (b) level 2 (c) level 5 ($Kn_\infty = 0.025$; $Kn_{cc} = 1$; $\phi_0 = 1.05$).
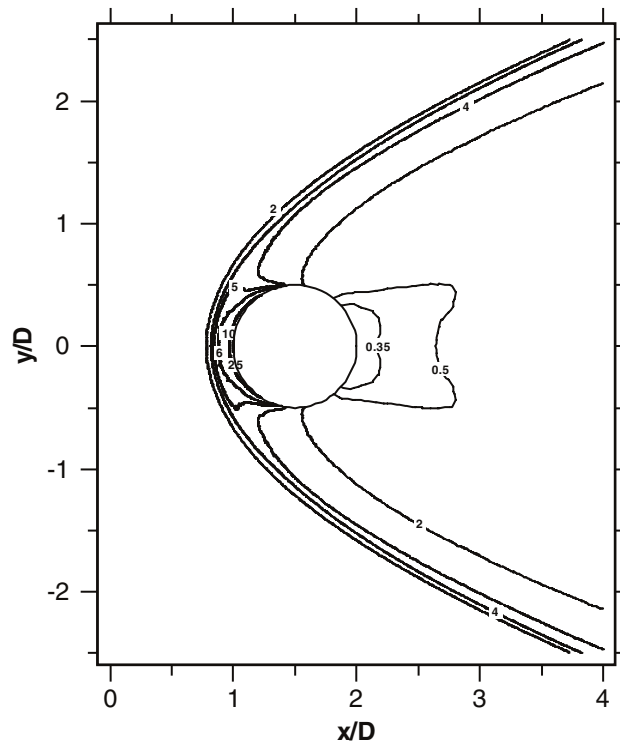
Figure 12. Normalised density ratio of a hypersonic flow over a cylinder using adaptive mesh ($Kn_\infty = 0.025$; 88 959 triangular cells).

ature non-equilibrium parameter becomes smaller far away from the cylinder and the shock. Thus, temperature non-equilibrium due to the complicated flow field is well resolved using the adaptive mesh.

Entropy contour Entropy in the flow domain is defined as

$$S = \frac{p/p_\infty}{(\rho/\rho_\infty)^r} - 1 \tag{4}$$

Where ρ/ρ_∞ and p/p_∞ represent the normalised pressure and density ratio, respectively. Figure 14 illustrates the entropy contour in the flow along with some typical streamlines. Following the streamlines far from the cylinder, the entropy generation is positive due to the compression wave but relatively small across the shock. After the shock, it becomes negative due to expansion and finally becomes essentially zero (isentropic) along the streamlines. It is, however, much larger across the shock near the cylinder due to the strong normal shock in the stagnation region. Considering the streamlines close to the stagnation line, we find that the entropy increases first across the shock, and then decreases in crossing the boundary layer of the cylinder. Later it increases again due to viscous dissipation in the boundary layer, and
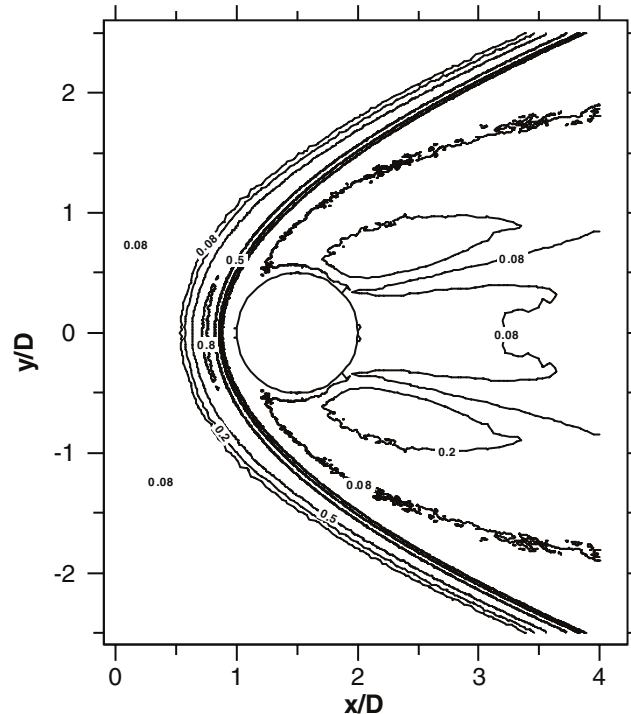
Figure 13. Non-equilibrium between translational and rotational temperatures for a hypersonic flow over a cylinder ($Kn_\infty = 0.025$; 88 959 triangular cells).

finally increases afterwards because of appreciable non-equilibrium in the wake region and the shear layer region.

Properties along the stagnation line Results of normalised number density (n/n_∞), and normalised translational and rotational temperatures (($T - T_\infty)/(T_o - T_\infty)$)) along the stagnation line are presented in Figures 15 and 16, respectively. Previous experimental data of Bütefisch [26] and DSMC data of Koura and Takahira [27] are also included in these figures for comparison. Table III summarizes the comparison of simulation parameters between the current study and Koura and Takahira [27]. First, for the density ratio, the present data agree well with both the available experimental data and simulated data in front of and behind the cylinder. The maximum density ratio (~ 23) of the present study is, however, larger than that (~ 16) of Koura and Takahira [27] due to the highly refined mesh in the stagnation region. Second, for the translational temperatures along the stagnation line, the current simulation data compare reasonable well with those of Koura and Takahira [27] (no experimental data is available). However, we find that the translational temperatures increase more rapidly to the peak value (1.2) but decrease at essentially the same rate to the stagnation value (0.25). The present simulate that data are in good agreement with those of Reference [27] in the wake region. Finally, for the rotational temperatures along the stagnation line, our data seems to
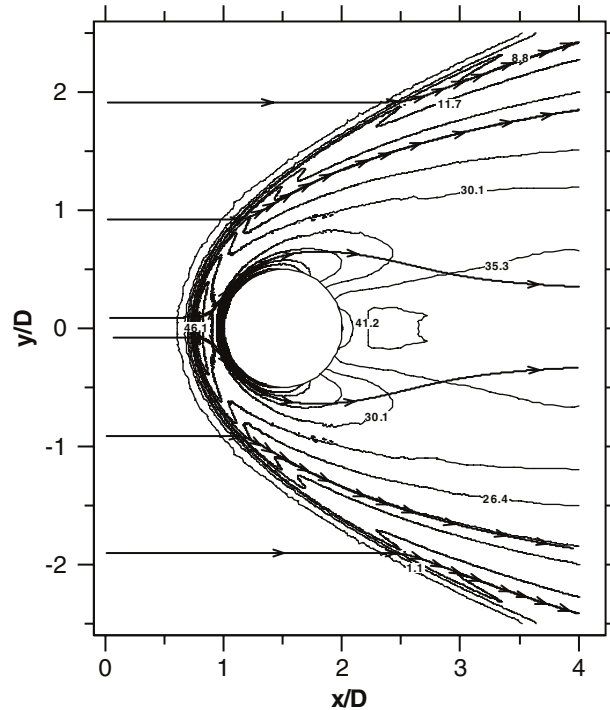
Figure 14. Entropy contour and typical streamlines for a hypersonic flow over a cylinder
($Kn_\infty = 0.025$; 88 959 triangular cells).

agree better with experimental data, especially in the stagnation point, than those of Koura and Takahira [27]. This should be also attributed to the highly refined mesh in the stagnation region.

V. CONCLUSIONS

In the current study, a DSMC method using the adaptive unstructured mesh is proposed. In this method, an isotropic mesh refinement is used to enrich the cell where the adaptation parameter, Kn_c, is smaller than the preset value. Additional constraint, $\phi > \phi_0$, is used in external flow to help reduce the total refined cell numbers by relaxing the adaptation criteria in the free-stream cells. An an-isotropic mesh refinement is then used to remove the hanging nodes in the interfacial cells, which are created during the isotropic refinement process. A high-speed driven cavity flow is used to verify the proposed method. Results all show that the current method of mesh adaptation using unstructured mesh is efficient and more accurate as compared with that without mesh adaptation. Finally, the developed method of mesh adaptation is applied to a hypersonic flow over a cylinder. Results are in good agreement with previous experimental and simulation data.
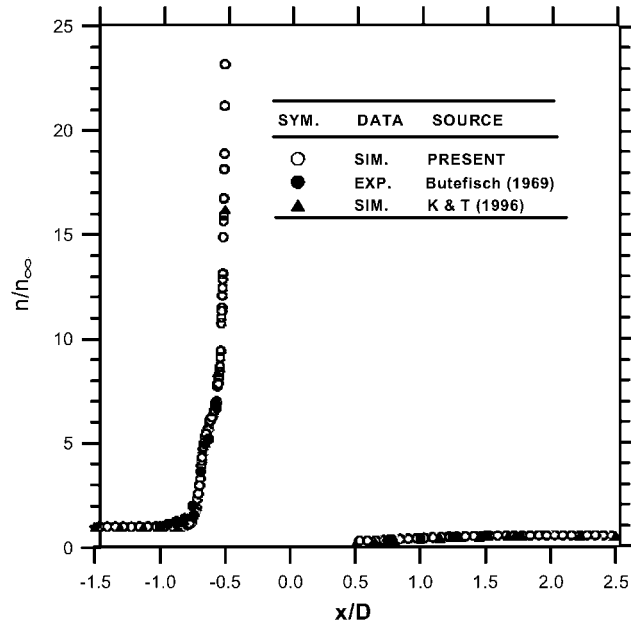
Figure 15. Normalised number density along the stagnation line for a hypersonic flow over a cylinder ($Kn_\infty = 0.025$; 88 959 triangular cells).
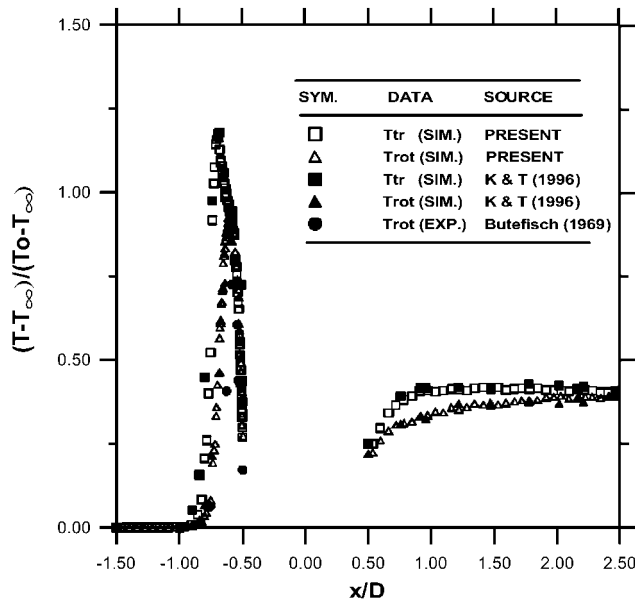

Figure 16. Normalised translational and rotational temperature along the stagnation line for a hypersonic flow over a cylinder ($Kn_\infty = 0.025$; 88 959).

Table III. Comparison of simulation parameters between the present study and Koura and Takahira [27].

	Present	Koura and Takahira [1994]
Model	VHS	VSS
Particle no.	3.7E5	1.E6
Rotational energy model	Parker	Parker
Mesh adaptation	Yes	No

In summary, major findings of the current research are listed as follows.

1. A mesh adaptation method (*h-refinement*) using unstructured mesh, combining the DSMC method, is proposed and tested successfully using a high-speed driven cavity flow as the benchmark problem.
2. The proposed method alleviates the burden often required on creating a suitable mesh considering the solution variations, which is generally not known *a priori*. It automatically generates a solution-based mesh in the current proposed method.
3. Application of the proposed method to a realistic hypersonic flow shows that the solution-based adaptive mesh can resolve several important flow features, e.g., shock.

Extension of the current mesh adaptation procedures to an unsteady flow problem is possible. However, not only the cell-refining process developed in the current study but also the cell-coarsening process has to be included. This will definitely complicate the mesh adaptation process. Practically, DSMC is rarely applied to compute the unsteady problem. In addition, it is well known that the computational cost of computing near-continuum gas flows using DSMC is prohibitively high even with current highly developed computers. One of the remedies is to take advantage of the parallelism inhered in the DSMC method. Thus, combining the mesh adaptation and parallel DSMC should help alleviate this problem greatly. The results, which take advantage of both, will be reported in the very near future.

REFERENCES

1. Schaff S, Chambre P. *Fundamentals of Gas Dynamics*. Princeton University Press: Princeton, NJ, 1958, Ch. H.
2. Bird GA. *Molecular Gas Dynamics*. Clarendon Press: Oxford, 1976.
3. Boyd ID, Jafry Y, Beukel JW. Particle simulation of helium microthruster flows. *Journal of Spacecraft Rockets* 1994; **31**:271–281.
4. Kannenberg KC. Computational method for the direct simulation Monte Carlo technique with application to plume impingement. Ph.D. Thesis. Cornell University, Ithaca, NY, 1998.
5. Lee YK, Lee JW. Direct simulation of compression characteristics for a simple drag pump model. *Vacuum* 1996; **47**:807–809.
6. Lee YK, Lee JW. Direct simulation of pumping characteristics for a model diffusion pump. *Vacuum* 1996; **47**:297–306.
7. Wu JS, Lee WS. Conductance computation of a short tube using the direct simulation Monte Carlo method. Submitted for publication.

8. Alexander FJ, Garcia AL, Alder BJ. Direct simulation Monte Carlo for thin-film bearings. *Physics of Fluids A* 1994; **6**:3854–3860.
9. Piekos ES, Breuer KS. Numerical modelling of micromechanical devices using the direct simulation Monte Carlo method. *Transactions of ASME Journal of Fluids Engineering* 1996; **118**:464–469.
10. Nance RP, Hash DB, Hassan HA. Role of boundary conditions in Monte Carlo simulation of microelectromechanical systems. *Journal of Thermophysics and Heat Transfer* 1998; **12** (technical notes): 447–449.
11. Wu JS, Tseng KC. Analysis of micro-scale gas flows with pressure boundaries using direct simulation Monte Carlo method. *Computers & Fluids* 2001; **30**:711–735.
12. Bird GA. *Molecular Gas Dynamics and the Direct Simulation of Gas Flows.* Oxford University Press: New York, 1994.
13. Merkle CL. New possibilities and applications of Monte Carlo methods. *Rarefied Gas Dynamics*, Belotserkovsk II (eds); 13th International Symposium on Rarefied Gas Dynamics, 1985; 333–348.
14. Shimada T, Abe T. Applicability of the direct simulation Monte Carlo method in a body-fitted coordinate system. *Rarefied Gas Dynamics*, Muntz *et al.* (eds). Progress in Astronautics and Aeronautics, AIAA 1989, 258–270.
15. Olynick DP, Moss JN, Hassan HA. Grid generation and application for the direct simulation Monte Carlo method to the full shuttle geometry. *AIAA Paper* 90-1692.
16. Powell KG, Roe PL, Quirk J. Adaptive mesh algorithms for computational fluid dynamics. *Algorithmic Trends in Computational Fluid Dynamics*. Springer Verlag: New York, 1992; 303–337.
17. Rausch RD, Batina JT, Yang HTY. Spatial adaptation procedures on unstructured meshes for accurate unsteady aerodynamics flow computation. *AIAA Paper* 91-1106.
18. Connell SD, Holms DG. Three-dimensional unstructured adaptive multigrid scheme for the Euler equations. *AIAA Journal* 1994; **32**:1626–1632.
19. Kallinderis Y, Vijayan P. Adaptive refinement-coarsening scheme for three-dimensional unstructured meshes. *AIAA Journal* 1993; **31**:1440–1447.
20. Wang L, Harvey JK. The application of adaptive unstructured grid technique to the computation of rarefied hypersonic flows using the DSMC method. *Rarefied Gas Dynamics*, Harvey J, Lord G (eds). 19th International Symposium, 1994; 843–849.
21. Robinson CD. Particle simulations on parallel computers with dynamic load balancing. PhD Thesis. Imperial College of Science, Technology and Medicine, UK, 1998.
22. Bohdan ZC. Combining the monotonic Lagrangian grid with a direct simulation Monte Carlo model. *Journal of Computational Phys.* 1995; **122**:323–334.
23. Alejandro LG, John B. Adaptive mesh and algorithm refinement using direct simulation Monte Carlo. *Journal of Computational Physics* 1999; **154**:134–155.
24. Lohern R, Parikh P. Generation of three-dimensional unstructured grids by advancing front method. *AIAA paper* 88-0515.
25. Baker T. Unstructured meshes and surface fidelity for complex shapes. In AIAA 10th Computational Fluid Dynamics Conference, 1991.
26. Bütefisch K. Investigation of hypersonic non-equilibrium rarefied gas flow around a circular cylinder by the electron beam technique. *Rarefied Gas Dynamics II*. Academic Press: New York, 1969; 1739–1748.
27. Koura K, Takahira M. Monte Carlo simulation of hypersonic rarefied nitrogen flow around a circular cylinder. Rarefied Gas Dynamics, 19th International Symposium, 1994; 1236–1242.